Chemistry & Biology
Article

Structure-Based Design of a Superagonist Ligand for the Vitamin D Nuclear Receptor

Shinji Hourai,[1,5] Luis Cezar Rodrigues,[4] Pierre Antony,[1] Bernardo Reina-San-Martin,[2] Fabrice Ciesielski,[1] Benjamin Claude Magnier,[3] Kristina Schoonjans,[3] Antonio Mouriño,[4] Natacha Rochel,[1] and Dino Moras[1,*]
[1]Institut de Génétique et de Biologie Moléculaire et Cellulaire, Département de Biologie et de Génomique Structurales, Université Louis Pasteur, Strasbourg F-67000, France
[2]Département de Biologie du Cancer, Inserm, U596
[3]Département de Neurobiologie et Génétique, CNRS, UMR7104
Illkirch, F-67400 France
[4]Universidad de Santiago de Compostela, Departamento de Química Orgánica and Unidad Asociada al CSIC, 15782, Spain
[5]Present address: Dainippon Sumitomo Pharma Co., Ltd., Genomic Science Laboratories, 3-1-98, Kasugadenaka, Konohanaku, Osaka 554-0022, Japan.
*Correspondence: moras@igbmc.u-strasbg.fr
DOI 10.1016/j.chembiol.2008.03.016

SUMMARY

Vitamin D nuclear receptor (VDR), a ligand-dependent transcriptional regulator, is an important target for multiple clinical applications, such as osteoporosis and cancer. Since exacerbated increase of calcium serum level is currently associated with VDR ligands action, superagonists with low calcium serum levels have been developed. Based on the crystal structures of human VDR (hVDR) bound to 1α,25-dihydroxyvitamin D_3 and superagonists—notably, KH1060—we designed a superagonist ligand. In order to optimize the aliphatic side chain conformation with a subsequent entropy benefit, we incorporated an oxolane ring and generated two stereo diasteromers, AMCR277A and AMCR277B. Only AMCR277A exhibits superagonist activity in vitro, but is as calcemic in vivo as the natural ligand. The crystal structures of the complexes between the ligand binding domain of hVDR and these ligands provide a rational approach to the design of more potent superagonist ligands for potential clinical application.

INTRODUCTION

The lipid soluble seco-steroid 1α,25-dihydroxyvitamin D_3 (1α,25$(OH)_2D_3$), or calcitriol, regulates multiple biological functions, including, cell growth, differentiation, antiproliferation, apoptosis, adaptive/innate immune responses, bone mineralization, and calcium/phosphate homeostasis. 1α,25$(OH)_2D_3$, or its analogs action, is achieved through the binding to its cognate nuclear vitamin D receptor (VDR), which belongs to the superfamily of steroid/thyroid hormone/retinoid nuclear receptors (NR) (Laudet and Gronemeyer, 2002). A striking feature of VDR arises from its various anatomical localizations encompassing skin, brain, heart, pancreas, kidney, intestine, colon, prostate, ovary, and breast (Banerjee and Chatterjee, 2003). Consequently, deregulation of VDR action, due to either mutation(s) in the encoding gene or impairment of VDR-mediated specific signals, may lead to severe diseases, such as cancers, psoriasis, rickets, renal osteodystrophy, and autoimmunity (multiple sclerosis, rheumatoid arthritis, inflammatory bowel diseases, type I diabetes; Bouillon et al., 2006; Holick, 2003; Ebert et al., 2006). Thus, VDR is an exquisite therapeutic target to potentially cure patients (Campbell and Adorini, 2006). However, routine use of 1α,25$(OH)_2D_3$ for clinical applications is hampered by its intrinsic hypercalemic/hypercalciuric character. To minimize this side effect, chemical modifications have been made on the A and/or CD rings or aliphatic chain of the natural ligand to generate apparently new analogs that were expected to exhibit marked hypocalcemic/hypocalciuric properties, while maintaining antiproliferative properties (Verlinden et al., 2000; Bouillon et al., 2005; Nagpal et al., 2005). Therefore, chemical synthesis of new 1α,25$(OH)_2D_3$ superagonists is on the leading edge of pharmaceutical research to eradicate the potential calcification of soft tissue from patients who have been subjected to chronic administration of 1α,25$(OH)_2D_3$ (Cheskis et al., 2006). With the aim of fulfilling these biological parameters, vitamin D superagonist analogs have been engineered, which are able to mediate transcriptional activity with a magnitude at least 10-fold higher than the natural ligand.

1α,25$(OH)_2D_3$, or its synthetic analogs bound to VDR, directs genomic outcomes preferentially as a heterodimer with its obligate partner, retinoid acid X receptor on response element located in the promoter regions of target genes (Carlberg and Dunlop, 2006). This specific binding modulates the production of ARN messenger (transcription) via the interaction with, a multi-component protein complex, which comprises functional coactivators or repressors, and the basal transcriptional machinery (Lonard and O'Malley, 2006). VDR activation with 1α,25$(OH)_2D_3$ induces its association with the p160 steroid coactivator (SRC) (Onate et al., 1995), cointegrators that remodel chromatin and mediator complexes (vitamin D interacting protein) which recruit RNA polymerase to efficiently achieve the initiation of the transcription, a highly dynamic and orderly regulated process (Rachez et al., 1999). As a member of the NR superfamily of transcription factors, VDR harbors a DNA binding domain and a ligand binding domain (LBD) (Laudet and Gronemeyer, 2002).

The LBD exerts a crucial regulatory function, because it contains both the ligand binding pocket (LBP) and the ligand-dependent transactivation function (AF-2).

Determination of three-dimensional structures of unliganded or liganded NR, as well as targeted NR mutagenesis, have highlighted that LBD undergoes a dramatic conformational change in response to specific ligand binding (Bourguet et al., 1995; Renaud et al., 1995). This induced-fit mechanism (mousetrap) is characterized by the folding back of H12 onto the core of LBD, thereby creating a hydrophobic cleft together with surface-exposed residues to facilitate the recruitment of coactivators, concomitantly with the release of corepressors. Resolution at the atomic level of the ligand-VDR LBD contacts has already provided significant insights into the structure-function relationship of the complex (Rochel and Moras, 2006; Yamada et al., 2003). We previously engineered a VDR LBD that lacks a flexible insertion domain between helices H1 and H3, and the resulting mutant bound to $1\alpha,25(OH)_2D_3$ exhibits similar conformation, transactivation ability, and biophysical properties compared to the wild-type counterpart (Rochel et al., 2000, 2001). Using this information, we have solved the crystal structure of human VDR (hVDR) in complex with $1\alpha,25(OH)_2D_3$ agonists, calcipotriol and seocalcitol (Tocchini-Valentini et al., 2004), and shown that the hVDR LBD complexes adopt the canonical conformation of all previously reported agonist-bound NR LBD (Rochel and Moras, 2006); indeed, helix 12 position and conformation are strictly maintained. Similar observations have been made for some synthetic analogs of $1\alpha,25(OH)_2D_3$ that exhibit superagonist properties, such as 14-epi analogs of vitamin D, 19-nor-14-epi-23-yne-$1\alpha,25(OH)_2D_3$ (TX522) and 19-nor-14,20-bisepi-23-yne-$1\alpha,25(OH)_2D_3$ (TX527), as well as 20-epi-analogs of $1\alpha,25(OH)_2D_3$, (MC1288) and 20-epi-22-oxa-24a,26a,27α-trihomo-$11\alpha,25(OH)_2D_3$ (KH1060) (Eelen et al., 2005; Tocchini-Valentini et al., 2001). These compounds are at least 10 times more potent in transactivation assays, and act as antiproliferative agents with a magnitude of several orders higher than $1\alpha,25(OH)_2D_3$ in vitro (Peleg et al., 1995). In all cases, the ligand is rather tightly bound to the receptor around the A, Seco B, C, and D rings. In contrast, the 17β-aliphatic side chain is less constrained (Eelen et al., 2005). Based on these observations, we propose that a superagonist analog could be designed by constraining the ligand conformation and strengthening the intermolecular contacts of the aliphatic side chain with the VDR LBP.

In this article, we describe the successful structure-based design of novel analogs of vitamin D. In order to optimize the aliphatic side chain conformation with a subsequent entropy benefit, we incorporated an oxolane ring and synthesized two stereo diasteroisomers, AMCR277A(C23S) and AMCR277B(C23R), with opposite stereochemistry at C23 of the oxolane moiety. We solved the crystal structure of hVDR LBD bound to each analog. In vitro and in vivo studies showed a drastic difference between the biochemical/biological effects of AMCR277A versus AMCR277B, compared with those induced by $1\alpha,25(OH)_2D_3$. The crystal structures provide an explanation for the superagonist activity mechanism of this compound and a rational approach to designing more potent ligands, which may serve for direct clinical applications and/or lead to the identification of new therapeutic targets.

RESULTS

Structure-Based Design of Novel Side Chain Analogs

In the crystal structures of VDR complexed with several agonist ligands, the ligand is tightly bound to the receptor around the A, Seco B, C, and D rings (Figure 1A; Rochel et al., 2000; Tocchini-Valentini et al., 2001, 2004; Eelen et al., 2005). In contrast, the aliphatic side chain is less constrained, thus allowing alternative conformations of the side chain for the $1\alpha,25(OH)_2D_3$ and the 20-epi analogs (Figure 1B). A correlation could be made between the number of favorable intermolecular contacts of aliphatic side chains with the LBP and the stability of the complex.

Superimposition of the side chain conformations of the VDR-ligand complexes KH1060 and $1\alpha,25(OH)_2D_3$ shows that the two lateral side chains exactly coincide, except at the C17 and C23 positions, where the two directions form a virtual heterocycle (Figure 1B). Based on this structural information, we designed a novel ligand that would incorporate a rigid ring system to minimize the entropic loss and maximize the number of protein-ligand contacts. To achieve this goal, the hybrid chemical structure of $1\alpha,25(OH)_2D_3$ and KH1060, incorporating a rigid ring with an oxolane moiety, was synthesized. Due to the chirality of the atom C23, two epimers were generated, AMCR277A and AMCR277B, with opposite stereochemistry at C23 of the oxolane moiety (Figure 1A). Preliminary docking experiments suggested that AMCR277A and $1\alpha,25(OH)_2D_3$ could adopt a similar conformation, and that additional O21 and C28 atoms made apparently new van der Waals contacts with the LBP (data not shown). On the other hand, AMCR277B should adopt a different conformation and induce a change in the protein structure. To test this hypothesis, we determined the crystal structures of the hVDR LBD complexes with AMCR277A and AMCR277B.

Chemical Synthesis of Two Apparently New Vitamin D Analogs, AMCR277A and AMCR277B

Synthesis of the targets compounds, AMCR277A and AMCR277B, is summarized in Figure 2, starting with ketone 1 (Fernández et al., 1992). The Lythgoe convergent approach was used for the construction of the vitamin D triene system by coupling ketone 2 with phosphine oxide 3 (Lythgoe, 1980; Kabat and Radinov, 2001; Mouriño et al., 1997). Detailed syntheses of both chemical compounds are reported in Figure S1 and elsewhere in the Supplemental Data available with this article online.

Ligand-Protein Interactions as Observed in the Crystal Structures

In the crystal structures of both complexes, the protein adopts the canonical conformation of all previously reported structures of VDR LBD bound to agonist and superagonist ligands with helix H12 folded in the agonistic position. Variations involve only some side chains located at the surface of the protein. When compared with VDR LBD-$1\alpha,25(OH)_2D_3$ complex, the atomic models show rmsd on the Cα atoms of 0.23 Å and 0.24 Å for VDR LBD-AMCR277A and VDR LBD-AMCR277B complexes, respectively.

Similar to the natural ligand, the analogs are encapsulated within the ligand pocket. AMCR277A and AMCR277B adopt an

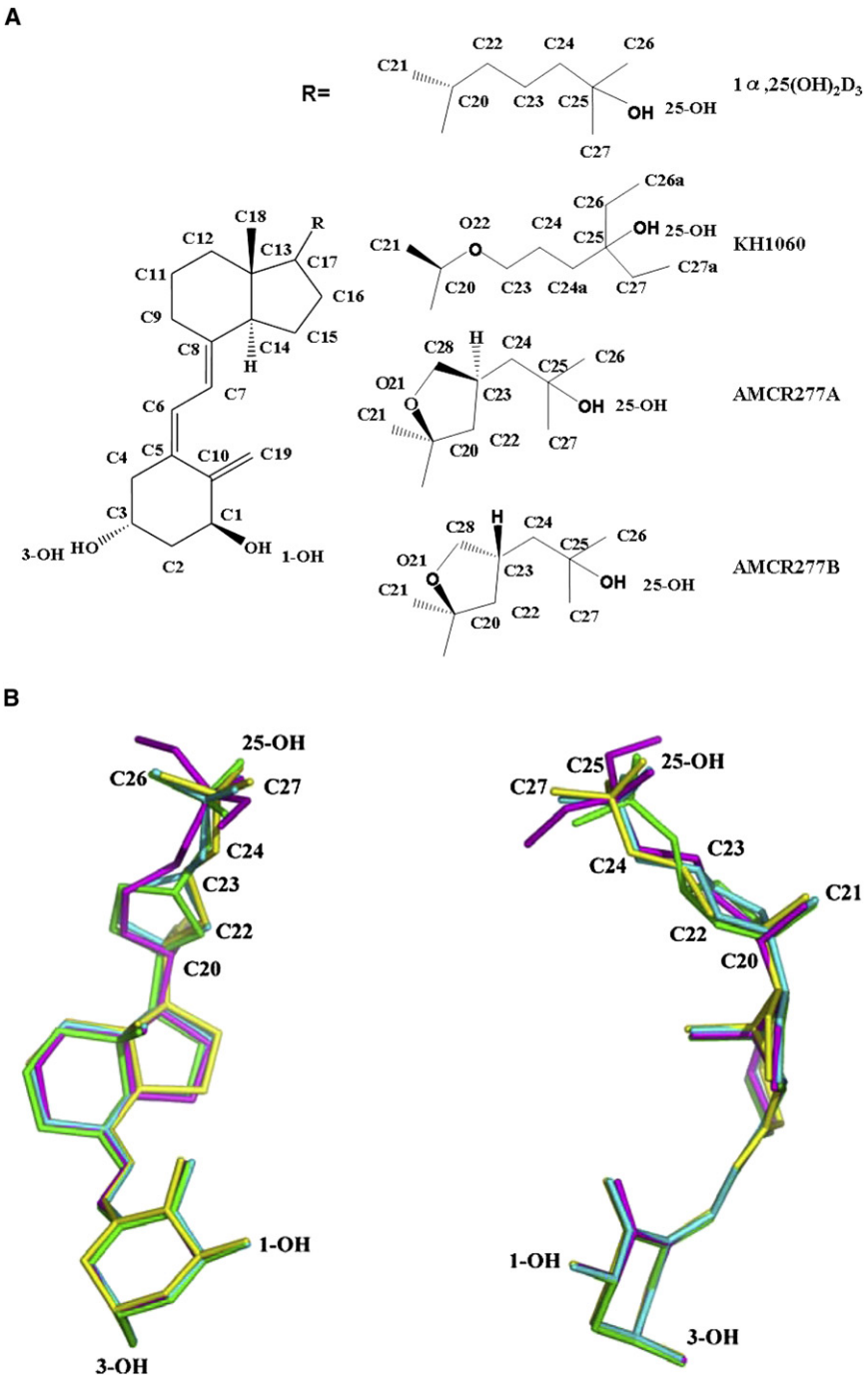

Figure 1. Chemical Structures and Conformation of the Bound Ligands 1α,25(OH)$_2$D$_3$, KH1060 and the Apparently New Ligands AMCR277A(C23S) and AMCR277B(23R)

(A) Chemical structures of 1α,25(OH)$_2$D$_3$, KH1060, AMCR277A, and AMCR277B are represented.

(B) Superposition of 1α,25(OH)$_2$D$_3$ (yellow), HK1060 (magenta), AMCR277A (cyan), and AMCR277B (green) after superimposed VDR complexes. Front (left) and side views (right) of the ligands are shown. Oxygen atoms are red. Atom numbers of 17β-aliphatic side chain and hydroxyl groups of 1α,25(OH)$_2$D$_3$ are shown. Coordinates are from 1DB1 (1α,25(OH)$_2$D$_3$) and 1IE8 (KH1060) from the Protein Data Bank.

elongated conformation, which is also observed in VDR LBD-1α,25(OH)$_2$D$_3$ and KH1060 complexes (Figures 1B and 3A). Thus, they form all previously observed contacts contributing to the tighter ligand-protein contacts. For all four complexes, the distance between 1-OH and 25-OH varies from 12.8 to 13.1 Å. The interactions between the protein and the A, Seco B, C, and D rings are identical, and the hydroxyl groups make the same hydrogen bonds: 1-OH with Ser-237 and Arg-274; 3-OH with Tyr-143 and Ser-278; and 25-OH with His-305 and His-397. Some specific contacts of the aliphatic side chains with VDR LBP are shown in Figure 3B (Val-300, His-305, His-397, Val-418). A novel feature when compared with 1α,25(OH)$_2$D$_3$ is the additional van der Waals contact of O21 with Val-300, which is also present but weaker in the VDR LBD-AMCR277B complex. This stronger interaction with Val-300 has also been observed in the VDR LBD crystal structures with the superagonist ligands KH1060 and TX522 (Tocchini-Valentini et al., 2004; Eelen et al., 2005). Due to the inverse configuration at C23, the stereoisomer AMCR277B adopts a different side chain conformation. C23 and C24 are 0.6 and 1.2 Å away, respectively, from their positions in the AMCR277A complex, thereby affecting their respective contacts. Consequently, the positions of C25, C26, C27, and 25-OH are also different, and the direct interaction of AMCR277B with activation helix 12 is then weaker (C27–Val-418 of 4.6 Å).

Relative Binding Affinity

The strength of the interaction of AMCR277A and AMCR277B for the hVDR LBD was evaluated by a comparative study against 1α,25(OH)$_2$D$_3$ with electrospray ionization mass spectrometry (ESI-MS) via the measure of their accelerating cone voltage needed to dissociate 50% of a noncovalent complex in the gas phase (Vc$_{50}$). The Vc$_{50}$ value reflects the electrostatic and hydrogen-bonding energies, and is currently used to study ligand binding strength (Rogniaux et al., 1999; El-Kabbani et al., 2000). Changes in electrostatic and H-bond contacts upon chemical modification of the ligand are directly reflected in the ESI-MS data, providing a qualitative classification of ligands similar to that obtained by classical competition experiments. The Vc$_{50}$ values of AMCR277A, AMCR277B, and 1α,25(OH)$_2$D$_3$ for the hVDR LBD were obtained from the ESI mass spectra (Figure S2). The Vc$_{50}$ values at which half of the species are liganded and half unliganded are 41, 39, and 38 V for AMCR277A, AMCR277B, and 1α,25(OH)$_2$D$_3$,

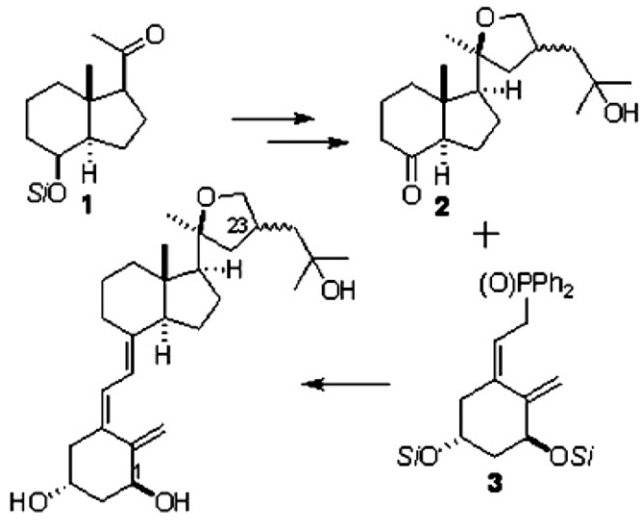

Figure 2. Summary of the Convergent Syntheses of the Targets Vitamin D_3 Analogs

Synthesis of the targets compounds AMCR277A(C23S) and AMCR277B(C23R) starts with the ketone 1. The Lythgoe convergent approach was used for the construction of the vitamin D triene system by coupling ketone 2 with phosphine oxide 3.

respectively, indicating a relative affinity for hVDR in the order of AMCR277A > AMCR277B ≈ 1α,25(OH)$_2$D$_3$. The higher affinity of AMCR277A is associated with increased contact, as shown in the crystal structure (Figure 3B).

To test the biological properties of AMCR277A and AMCR277B, in vitro and in vivo experiments were conducted by monitoring analog-induced transcriptional activity, cell proliferation arrest/differentiation, and calcium serum level.

AMRC277A and Not AMRC277B Activates Transcription at 0.1 nM

Previous studies with gene reporter assays have shown that vitamin D superagonists, including KH1060, have the potency to stimulate transcription at 100-fold lower concentration than the natural ligand. Here, inducible VDR-dependent transcriptional activity was quantified with EBNA 293 cells that were transiently cotransfected with a Gal4-VDR LBD expression vector and the UAS-TATA luciferase reporter construct. Consistent with previous findings, VDR-mediated transcription occurs in a dose-dependent manner with 1α,25(OH)$_2$D$_3$ (Figure 4A; Eelen et al., 2005). We now demonstrate that the analogs exhibit a drastic difference in their capacity to induce transcription. Indeed, we show that, at 0.1 nM, VDR LBP-dependent transcription activity is 12 times more potent with AMCR277A compared with AMCR277B or 1α,25(OH)$_2$D$_3$ (Figure 4A). At this concentration, the luciferase activity was barely detectable with AMCR277B or 1α,25(OH)$_2$D$_3$ as stimulatory agents. Up to a dose of 10 nM, the fold transcriptional induction was still significantly greater in the presence of AMCR277A. Thus, AMCR277A exhibits superagonist properties in mediating transcription, while AMCR277B acts as 1α,25(OH)$_2$D$_3$.

AMRC277A at 1 nM Induces HL60 Cell Proliferation Arrest and Differentiation In Vitro

Since AMCR277A is a superagonist and AMCR277B is not, we postulate that this biochemical effect may induce specific cell phenotype. To test this hypothesis, we used the human cell

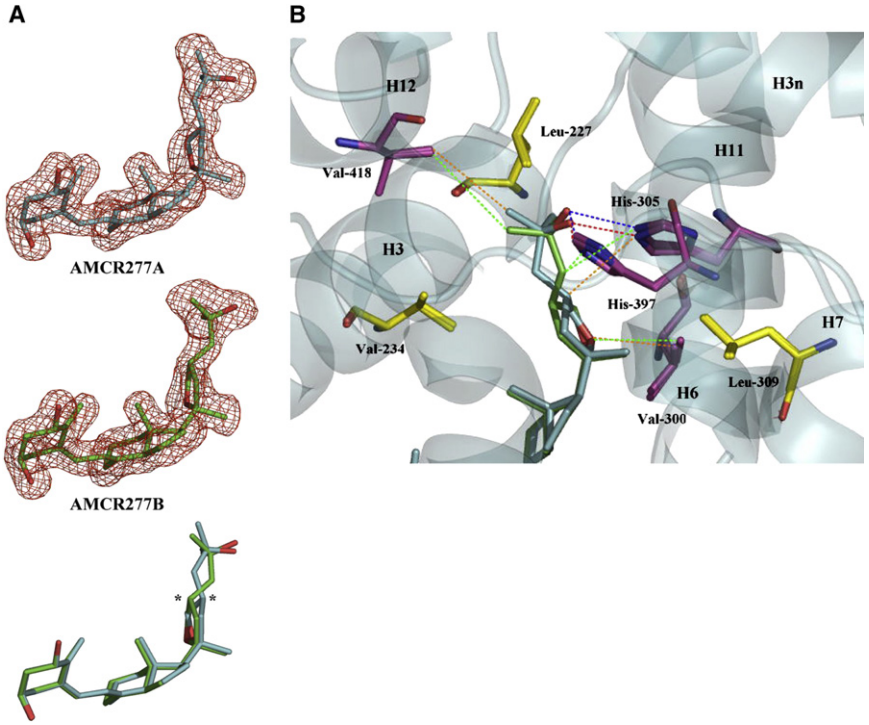

Figure 3. Detailed Structural Representation of Both Analogs Alone or Bound to hVDR LBD

(A) The δ_A-weighted $F_o - F_c$ omit map is shown contoured at 3.3 δ (red). AMCR277A (cyan) and AMCR277B (green) are shown in stick representation. Comparison of the ligand conformation of AMCR277A (cyan) and AMCR277B (green) are shown after superpimposition. Chiral carbon atom C23 is marked with asterisks. Oxygen atoms are colored red.

(B) Close-up view of AMCR277A and AMCR277B in the VDR LBP. AMCR277A and AMCR277B are shown in cyan and green, respectively. The residues, which are closer than 4.0 Å and important for comparison purposes, are shown in yellow. Specific residues involved in interactions are highlighted in magenta. Oxygen and nitrogen atoms are shown in red and blue, respectively. Hydrogen bonds of AMCR277A and AMCR277B complexes are shown in red and blue dotted lines, respectively. Van der Waals bonds of AMCR277A and AMCR277B complexes are shown in orange and green dotted lines, respectively. Secondary structure of VDR is shown in cyan; H3n, H3, H6, H7, H11, and H12 indicate helices.

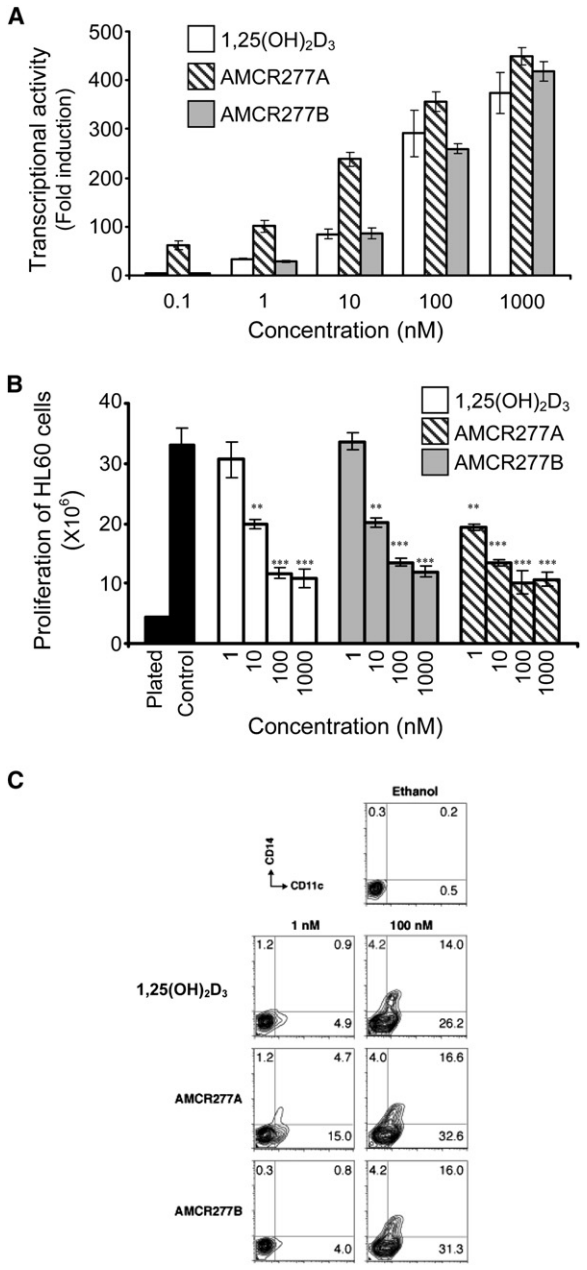

Figure 4. AMCR277A Acts as a Superagonist Molecule In Vitro

(A) AMCR277A, and not AMCR277B or $1\alpha,25(OH)_2D_3$, induces transcription activity at a dose of 0.1 nM. A total of 293 EBNA cells were transiently transfected with a UAS-TATA-luciferase reporter plasmid and an expression plasmid of Gal4 DBD-VDR LBD and subsequently treated with $1\alpha,25(OH)_2D_3$, AMCR277A, or AMCR277B. Luciferase activity for each sample was normalized to the β-galactosidase activity. Data are shown as fold induction of agonist-induced luciferase activity divided by luciferase activity of vehicle. Data are presented as mean ± SEM.

(B) AMCR277A-mediated HL60 cell growth arrest is achieved for a dose of 1 nM. HL60 cells were incubated for 96 hr with $1\alpha,25(OH)_2D_3$, AMCR277A or AMCR277B at various concentrations and counted. Data are presented as mean ± SEM. $^{**}p < 0.01$; $^{***}p < 0.001$.

(C) AMCR277A-mediated HL60 differentiation into monocyte-like cells is achieved for a dose of 1 nM. Cells were labeled with PE-labeled anti-human CD11c and FITC-labeled anti-human CD14, and HL60 cell differentiation was estimated by the double-positive CD11c/CD14 population. Data are representative of three distinct experiments.

clone HL60, because in vitro culture of HL60 cells in the presence of $1\alpha,25(OH)_2D_3$ induces proliferation arrest and triggers their differentiation into a monocyte-like phenotype characterized by the upregulation of surface marker expression of CD11c and CD14 (McCarthy et al., 1983; White et al., 2005). HL60 cells represent a genuine model for the study of the effects of $1\alpha,25(OH)_2D_3$ analogs on the clonal proliferation inhibition of fresh, acute myeloid leukemic cells harvested from patients (Pakkala et al., 1995). To determine whether the analogs display similar responses as the natural ligand, we cultured HL60 cells in vitro with increasing concentrations of AMCR277A, AMCR277B, or $1\alpha,25(OH)_2D_3$. We monitored proliferation arrest by live cell enumeration and determined their differentiation status by flow cytometry at different time points (Figures 4B and 4C). Our findings indicated that AMCR277B-treated HL60 cells led to a growth arrest comparable to $1\alpha,25(OH)_2D_3$ at all doses tested. In sharp contrast, a dose of only 1 nM of AMCR277A resulted in a 45% reduction in cell numbers, whereas no effect was observed with AMCR277B or $1\alpha,25(OH)_2D_3$. No significant difference in ligand-induced proliferation arrest was detected for concentrations higher than 10 nM. Thus, analog AMCR277A leads to a 10-fold higher HL60 cell proliferation arrest than $1\alpha,25(OH)_2D_3$ or analog AMCR277B.

To test whether the analogs also induce differentiation of HL60 cells, we determined the surface expression level of CD14 and CD11c by flow cytometry after 96 hr in culture. Cell differentiation was achieved in the presence of $1\alpha,25(OH)_2D_3$ or the analogs (Figure 4C). No difference in the production of CDs was observed with 100 nM saturating concentration of agonists. Consistent with the increased proliferation arrest observed, AMCR277A displayed a higher capacity to induce the production of CD11c and CD14 when compared with $1\alpha,25(OH)_2D_3$ or AMCR277B at 1 nM. Here, we show that 20.9% of the HL60 cells express CD11c and/or CD14 upon 96 hr treatment with 1 nM of AMCR277A, while the percentage was only 7.0 and 5.1 with $1\alpha,25(OH)_2D_3$ and AMCR277B, respectively (Figure 3C). Moreover, a CD11c/CD14 double-positive HL60 subpopulation was observed only with AMCR277A as agonist, indicating that this specific stereoisomer is a better inducer of HL60 differentiation (Figure 4C).

AMCR277B Is Less Calcemic than $1\alpha,25(OH)_2D_3$ while AMCR277A Behaves Like $1\alpha,25(OH)_2D_3$ In Vivo

Systemic administration of most $1\alpha,25(OH)_2D_3$ analogs induces hypercalcemia, thereby limiting their use for therapeutic applications. A lower calcemic action of AMCR277A relative to that of the natural ligand would enhance its potential clinical role. Therefore, we examined the in vivo effect of $1\alpha,25(OH)_2D_3$ analogs by monitoring the level of calcium in the serum of male C57BL/6J mice that were subjected to intraperitoneal injections for 3 wk with 0.1 or 0.5 μg/kg AMCR277A, AMCR277B, or $1\alpha,25(OH)_2D_3$ versus vehicle.

All mice survived beyond 3 wk after analog treatments (data not shown). Like $1\alpha,25(OH)_2D_3$, both analogs induce increased calcium serum level in a dose-dependent manner. Our results

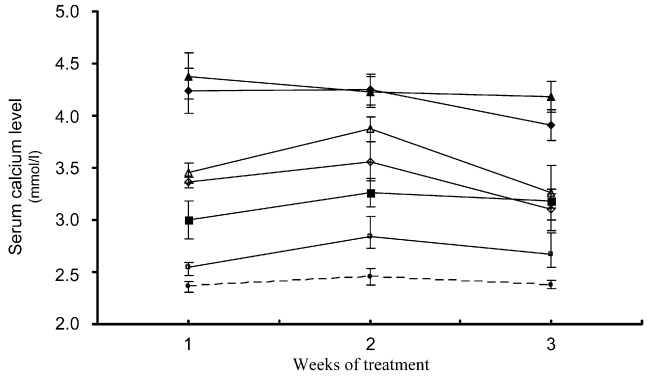

Figure 5. AMCR277B Is Less Calcemic than 1α,25(OH)$_2$D$_3$ while AMCR277A Behaves Like 1α,25(OH)$_2$D$_3$ In Vivo

Mice (1 wk-old; 6–7 mice/group) were injected intraperitoneally with 1α,25(OH)$_2$D$_3$, AMCR277A, AMCR277B, or sesame oil as diluent (vehicle) for 3 wk. Doses of analogs that were administrated were 0.1 and 0.5 μg/kg. Calcium serum level was monitored as described in the Experimental Procedures. Open circles, control; open triangles, AMCR277A 0.1 μg/kg; closed triangles, AMCR277A 0.5 μg/kg; open squares, AMCR277B 0.1 μg/kg; closed squares, AMCR277B 0.5 μg/kg; open diamonds, 1α,25(OH)$_2$D$_3$ 0.1 μg/kg; closed diamonds, 1α,25(OH)$_2$D$_3$ 0.5 μg/kg. Data are presented as mean ± SEM.

indicate that AMCR277A is as calcemic as 1α,25(OH)$_2$D$_3$ at 0.1 and 0.5 μg/kg, whereas AMCR277B is significantly less calcemic compared with the natural ligand (Figure 5).

DISCUSSION

In the present investigation, we designed a 1α,25(OH)$_2$D$_3$ ligand by incorporating an oxolane ring in the aliphatic side chain. As a result, we generated two 1α,25(OH)$_2$D$_3$ analogs with opposite stereochemistry at C23 of the oxolane moiety (Figure 1). We observed that, in vitro, AMCR277A(C23S) exhibits specific biological outcomes compared with AMCR277B(C23R) or 1α,25(OH)$_2$D$_3$ at two different levels: AMCR277A is a superagonist because it mediates transcription more than 10-fold higher than the natural ligand, and a low dose of AMCR277A significantly inhibits HL60 cell proliferation and further induces their differentiation into monocyte-like cells. However, in vivo studies indicate that AMCR277A-induced calcium serum increase is similar to that obtained with the natural ligand.

The two crystal structures provide an explanation for the higher transactivation potency of AMCR277A (Figures 1B, 3, and 4A). In this case, the oxolane ring stabilizes a conformation that mimics the bound form of the natural ligand, adopting the energetically favorable half-boat conformation that allows the side chain to fit without further tension as shown in the observed bond angle of C23-C24-C25 (118°), similar to those of 1α,25(OH)$_2$D$_3$ (121°) and KH1060 (118°). Further stability is also provided by the additional van der Waals contact of O21 with Val-300 (H6). This additional contact with Val-300 is also observed in the complexes formed between VDR and the superagonists KH1060 and TX522, but is absent in the complex with the 20-epi-1α,25(OH)$_2$D$_3$, for which closer contacts with His-305 and His-397 are observed (Eelen et al., 2005; Tocchini-Valentini et al., 2001). In contrast to AMCR277B, the additional van der Waals contacts with the LBP are compensated by the energetically unfavorable planar conformation of the oxolane ring (torsion angles of O21-C20-C22-C23 and C20-C22-C23-C28 are −9° and −3°, respectively), the larger C23-C24-C25 bond angle (124°), and the weaker interaction of C27 with Val-418 of H12. The apparently new ring fulfills two functions: a larger fraction of the LBP is occupied by the ligand, thus giving rise to additional stabilizing contacts, and the active form of the bound ligand is favored by the ring pucker. Stabilization of an energetically favorable bound conformation is equivalent to the selection of an optimal conformer within an ensemble, and has clear entropic advantages for an induced-fit process (Norman et al., 2004). This should affect the ligand specificity as well as the binding kinetics. This stabilized conformation is essential and specific for VDR-mediated transcription in the presence of AMCR277A, because the luciferase activity was similar and very low with either AMCR277B or 1α,25(OH)$_2$D$_3$ (Figure 4A).

The specific 1α,25(OH)$_2$D$_3$ analogs-VDR interactions may also explain the ability of AMCR277A, and not 1α,25(OH)$_2$D$_3$ or AMCR277B, to inhibit HL60 cell proliferation at a dose of 1 nM (Figure 4C). It should be emphasized that a concentration of 10 nM AMCR277B or 1α,25(OH)$_2$D$_3$ is required to achieve similar biological effects as 1 nM of AMCR277A in directing HL60 phenotype (Figures 4B and 4C). Our results are consistent with previous findings demonstrating that a dose of 1 nM 1α,25(OH)$_2$D$_3$ is barely able to reduce HL60 cell growth (Pakkala et al., 1995). In contrast, KH1060, at a concentration even lower than 1 nM, is able to markedly decrease the division of HL60 cells. Indeed, soft agar culture experiments have shown that 0.1 nM KH1060 for 72 hr reduces the clonal expansion of HL60 cells by 50%. Consistent with previous findings, we found that 1 nM KH1060 for 96 hr fully differentiates HL60 cells (data not shown and Elstner et al., 1996). We now report that 1 nM of AMCR277A is 5-fold more efficient in inducing HL60 differentiation compared with AMCR277B or 1α,25(OH)$_2$D$_3$ (Figure 4C), highlighting its specific biological action. Since AMCR277A was designed based on the superimposition of the side chain conformations of the VDR LBD-ligand complexes KH1060 and 1α,25(OH)$_2$D$_3$, AMCR277A is likely to act as a marked antiproliferative molecule in human breast cancer in vitro, as observed with KH1060 in the estrogen-responsive MCF-7 adenocarcinoma cell line or the non-estrogen-responsive MDA-MB-231 malignant cells (Elstner et al., 1995). Further use of AMCR277A for clinical trials and therapeutics applications is contingent upon its efficiency to achieve physiological calcium serum level. Our in vivo experiments indicate that AMCR277A at 0.1 or 0.5 μg/kg is as calcemic as the natural ligand, whereas AMCR277B is less calcemic than 1α,25(OH)$_2$D$_3$. Although AMCR277A is a superagonist and an antiproliferative molecule, monitoring both cancer growth and calcemic effects in vivo will allow assessment of its selectivity. It should be emphasized that the biological activity of both analogs is likely to be contingent upon the oxidation at C-24 of their side chain as well as at C-3 of epimerization pathways. The generation of 24-oxo metabolites was not monitored in our study, but their potential production may lead, per se, to HL60 cell proliferation/differentiation, since 24-oxo metabolites of 16-ene and 20-epi analogs are as efficient as their parent analogs in directing cancer cell growth arrest (Reddy et al., 2007).

The present analysis suggests a possibility for further improvement of the potency and the specificity of the ligand. An easy way to increase the stability of the complex would be to fill up more of the LBP, leading to additional contacts between protein and ligand. A methylation at position C-2 would meet this requirement, since the crystal structure of VDR in complex with $1\alpha,25(OH)_2D_3$ shows an empty cavity at this location. Indeed, we recently solved the crystal structure of hVDR LBD complexes to 2α-methyl $1\alpha,25(OH)_2D_3$ and showed that the 2α-methyl group fills a small cavity in the LBD, making additional contacts with Phe-150, Leu-233, and Ser-237. These bonds are likely to explain the 4-fold increased affinity of the 2α-methyl-$1\alpha,25(OH)_2D_3$ for VDR and the 2.5-fold increase in inducing HL60 cell differentiation (Hourai et al., 2006). Therefore, the methylation at position C-2α of AMCR277A should further increase the superagonist feature of the ligands. The structure-based design of novel side chain analogs provides a rational explanation of superagonist activity. We can now compare the experimental information of several different but closely related molecules, with a broad spectrum of transactivation potencies, for which we solved the crystal structures (Rochel et al., 2000; Tocchini-Valentini et al., 2001, 2004; Eelen et al., 2005; Hourai et al., 2006; Ciesielski et al., 2007). The crystal structures of VDR-AMCR277A and VDR-AMCR277B complexes confirm earlier observations that the conformation of the receptor is not affected by superagonist ligands (Tocchini-Valentini et al., 2004; Eelen et al., 2005; Vanhooke et al., 2004). The superagonistic activity of AMCR277A can be explained by a combination of enthalpic effects (additional and tighter intermolecular contacts due to the higher fraction of LBP being occupied) and entropic effects (energetically favorable, preformed conformations), resulting in an overall gain both in binding energy and kinetics. All these factors contribute to a better specificity of the ligand for VDR. Further structure-based design of even more potent and specific ligands on the basis of these structural data can be considered.

In summary, we have generated, to our knowledge, the first structure-based $1\alpha,25(OH)_2D_3$ superagonist analog, AMCR277A(C23S). The combination of cell-based assays and structural analysis showed that this compound is a potent superagonist that may serve as a template for the design of even more efficient superagonists to be used for clinical applications to treat various types of cancer, including those of the breast and blood. However, AMCR277A behaves like the natural ligand in terms of calcemia, preventing its use in vivo. Based on these data, incorporation of an oxolane ring in the aliphatic side chain associated with specific chemical modifications at the C2α of the A ring is expected to improve the capacity of new analogs to significantly reduce cell mitosis of malignant cells in vivo. Compelling evidence has shown that selected, substituted $1\alpha,25(OH)_2D_3$ agonists orchestrate the finely tuned recruitment of specific coactivators (as well as the release of corepressors) to the VDR to induce chromatin remodeling, facilitating the initiation of transcription (Banerjee and Chatterjee, 2003). We postulate that the multiprotein complex scaffold directs the subsequent transcriptional program and gene activation, in a temporal-regulated manner, which lead to a specific biological outcome, including HL60 cell growth arrest. The molecular mechanisms underlying the serum calcium level that may result from rapid (nongenomic) or sustained (genomic) effects is still a matter of debate. Deciphering the structural and molecular mechanisms that explain the dissociation between the VDR-mediated genomic effects from the calcemic effects is expected to unravel new therapeutic targets and facilitate the design of more potent superagonists.

SIGNIFICANCE

Vitamin D nuclear receptor (VDR) acts as a ligand-dependent transcription to control multiple biological responses, including cellular antiproliferation, immune responses, and bone mineralization. Intrinsic effects of $1\alpha,25$-dihydroxyvitamin D_3 ($1\alpha,25(OH)_2D_3$)-mediated signal action are characterized by exacerbated increase of calcium serum levels, which limits its use for therapeutics applications. Numerous $1\alpha,25(OH)_2D_3$ analogs have been synthesized, but only a few display significant clinical relevance. Therefore, the generation of new VDR ligands, based on the knowledge of the crystal structure of VDR bound to its natural ligand, that exhibit low calcemic side effects and/or antitumoral properties, is the topic of intensive research in the pharmaceutical industry.

The present study reports the structure-based design of a novel VDR superagonist ligand, its chemical synthesis, and, to our knowledge, the first in vitro and in vivo tests. In order to optimize the aliphatic side chain conformation, we incorporated an oxolane ring between C17 and C23 of the side chain and generated two $1\alpha,25(OH)_2D_3$ analogs, AMCR277A(C23S) and AMCR277B(C23R), with opposite stereochemistry at C23 of the oxolane moiety. We solved the crystal structure of the ligand binding domain of the human VDR liganded to each compound and determined that the oxolane conformation is energetically more favorable for AMCR277A compared with AMCR277B. Transcriptional assays show that AMCR277A is a VDR superagonist, whereas AMCR277B behaves like the natural ligand. This specific property of AMCR277A is associated with a more potent ability to reduce HL60 cell proliferation. However, AMCR277A administration to mice, but not that of AMCR277B, is as calcemic as the natural ligand. The crystal structures provide an explanation for the superagonist activity mechanism of this compound and a rational approach to the design of more potent ligands, which may serve for direct clinical applications and/or lead to the identification of new therapeutic targets.

EXPERIMENTAL PROCEDURES

Synthesis of AMCR277A(C23S) and AMCR277B(23R)

The detailed synthesis of AMCR277A and AMCR277B are described in the Supplemental Experimental Procedures and Figure S1.

Purification and Crystallization

Crystals of the hVDR LBD in complexes with AMCR277A and AMCR277B were obtained with the mutant lacking 50 residues in the loop connecting helices H1 and H3, used to solve the structure of the VDR LBD bound to $1\alpha,25(OH)_2D_3$ and several synthetic ligands (Rochel et al., 2000; Tocchini-Valentini et al., 2001, 2004; Eelen et al., 2005; Hourai et al., 2006). Purification and crystallization of hVDR LBD complexes with the apparently new ligands

were carried out by the previously described procedure (Rochel et al., 2000, 2001). Briefly, the LBD of hVDR (residues 118–427 [delta] 165–215) was cloned in pET28b expression vector to obtain an N-terminal hexahistidine-tagged fusion protein, and was overproduced in *Escherichia Coli* BL21 (DE3). Cells were grown in LB medium and subsequently induced for 6 hr at 20°C with 1 mM isopropyl thio-β-D-galactoside. Protein purification included a metal affinity chromatography step on a cobalt-chelating resin. The tag was removed with thrombin and the protein further purified by gel filtration. The final protein buffer was 10 mM Tris (pH 7.5), 100 mM NaCl, and 5 mM dithiothreitol. The protein was concentrated to 10 mg/ml and incubated in the presence of a 5-fold excess of the ligands. The purity and homogeneity of the protein were assessed by SDS-PAGE and native-PAGE. Crystals of the complexes were obtained at 4°C by vapor diffusion in hanging drops. Crystals of VDR LBD-1α,25$(OH)_2D_3$ complex were used for microseeding, and the seeds from serial dilutions were introduced into freshly made drops. The reservoir solutions contained 100 mM MES-KOH and 1.4 M ammonium sulfate at pH 6.0.

X-Ray Data Collection and Structure Determination

The crystals were cryoprotected with a solution containing the reservoir solution plus 30% glycerol and 5% PEG400, mounted in fiber loops and flash cooled in liquid ethane at liquid N_2 temperature. Data collection from a single frozen crystal was performed at 100K at the beamline BM30 of the ESRF (Grenoble, France). The crystals were isomorphous and belonged to the orthorhombic space group $P2_12_12_1$ with the unit cell parameters as specified in Table 1. Data were integrated and scaled with the HKL2000 program package (Otwinowski and Minor, 1997).

The crystal structures of the VDR LBD complexes with AMCR277A and AMCR277B were solved by molecular replacement by using the known hVDR LBD-1α,25$(OH)_2D_3$ structure as a starting model and refined at 2.0 and 1.8 Å resolution, respectively. The omit maps from the refined atomic model of VDR LBD were used to fit the ligands to their electron density, as shown in Figure 3B. Anisotropic scaling and a bulk solvent correction and restrained isotropic atomic B-factor refinement were used. The average temperature factors for the ligands (14.3 and 14.1 $Å^2$ for AMCR277A and AMCR277B, respectively) were lower than those for proteins (23.2 and 18.3 $Å^2$ for AMCR277A and AMCR277B, respectively).

Alternate cycles of maximum likelihood refinement and model fitting were subsequently performed to generate the final models of the complexes. All data were included in the refinement (no δ cutoffs). All refined models showed unambiguous chirality for the ligands and no Ramachandran plot outliers according to PROCHECK. The final models of VDR-AMCR277A and VDR-AMCR277B complexes contained 255 residues, with no clear electron density for the first two N-terminal residues and the last four C-terminal residues, and poor electron density for residues 375–377 in the loop connecting H9-H10. Crystallographic data are summarized in Table 1. MOLREP, CNS-SOLVE, and O programs were used for molecular replacement, structure refinement, and model building (Vagin and Teplyakov, 2000; Brünger et al., 1998; Jones et al., 1991). For the structure comparison, Cα traces of the models were superimposed with the *lsq* commands of O and default parameters. Figures were generated with Pymol.

Transfection and Transactivation Assay

The hVDR LBD was subcloned into the pG4M-derived plasmid as a Gal fusion protein. Transient transfection experiments for the analysis of VDR activation were performed in 48-well plates by a standard calcium phosphate coprecipitation technique, as previously described (Rochel et al., 2001). A total of 293 EBNA cells were seeded (6.0×10^4 cells/well) and incubated for 24 hr at 37°C in DMEM containing 1g/l glucose, 10% fetal calf serum (FCS; Sigma), gentamycine (Kalys), and 1 mg/ml G418 (geneticin). The 293 EBNA cells were transiently transfected with 12.5 ng of Gal4-VDR LBD plasmid, 10 ng of UAS-TATA-luciferase reporter plasmid, and 37.5 ng of PCH110 internal control recombinant expressing β-galactoside plasmid. Cells were incubated for 8 hr at 37°C, then stimulated with the 1α,25$(OH)_2D_3$, AMCR277A, or AMCR277B for 20 hr at indicated concentrations in fresh medium, and washed with PBS prior to harvest in Passiv lysis buffer (Promega). Cell lysates were assayed for luciferase and β-galactosidase activity. Luciferase activity for each sample was normalized to β-galactosidase activity. All experiments were performed in duplicate.

Table 1. Data Collection and Refinement Statistics

Ligand	AMCR277A	AMCR277B
Wavelength (Å)	0.9794	0.9796
Space group	$P2_12_12_1$	$P2_12_12_1$
Cell dimensions (Å)		
A	45.01	45.06
B	51.37	51.46
C	132.24	132.13
Resolution range (last shell) (Å)	20–2.0 (2.07–2.0)	20–1.8 (1.86–1.8)
Unique reflections	21,276	28,589
Completeness (last shell) (%)	99.7 (97.8)	99.5 (97.3)
<I/δ(I)>	30.2 (5.7)	26.7 (4.2)
R_{merge} (last shell)[a]	0.062 (0.232)	0.061 (0.294)
R_{cryst} (%)[b]	18.6	19.2
R_{free} (%)[c]	21.7	20.6
Rmsd bond lengths (Å)	0.005	0.005
Rmsd bond angles (deg)	1.05	1.09
Nonhydrogen protein atoms	2019	2019
Nonhydrogen ligand atoms	32	32
Solvent molecules	159	193
Average B factor for nonhydrogen atoms ($Å^2$)		
Protein	23.2	18.3
Ligand	14.3	14.1
Solvent	32.5	28.1

[a] R_{merge}: $\Sigma|I_h - \langle I_h\rangle|/\Sigma I_h$, where I_h is the measurement of the intensity of reflection h and $\langle I_h\rangle$ is its mean value.
[b] R_{cryst}: $\Sigma||F_o| - |F_c||/\Sigma|F_o|$, where F_o and F_c are the observed and calculated structure factor amplitudes, respectively.
[c] R_{free} was calculated from 5% of all the data that were not used in the refinement.

Cell Culture and Differentiation

HL60 cells were cultured in complete RPMI with 10% FCS and 5% gentamycine at 37°C without CO_2, as described previously, and plated at a density of 4×10^5 cells/ml and cultured for 96 hr in the presence of 1α,25$(OH)_2D_3$, AMCR277A, or AMCR277B at concentrations ranging from 1 nM to 1 μM (White et al., 2005). As control, cells were incubated with 0.7% ethanol solution used to dissolve 1α,25$(OH)_2D_3$ and its analogs. Cells were counted with a hemocytometer, and dead cells were excluded by trypan blue staining. HL60 cell differentiation was determined by flow cytometry with PE-conjugated anti-human CD11c and FITC-conjugated anti-human CD14 antibodies (PharMingen/BD Biosciences). Topro-3 (Molecular Probes) was added immediately before laser excitation to exclude dead cells. Cells were analyzed on a FACSCalibur (Becton Dickinson) and with FlowJo software (TreeStar Inc.).

Mice and Serum Calcium Quantitation

Animal protocols were approved by the Alsace regional ethics committee. Male C57BL/6J mice were obtained from Charles River Laboratories, France (l'Arbresle, France). Mice (6–7 wk old) were maintained in a temperature-controlled (23°C) facility with a 12 hr light/dark cycle, and were given free access to food and water. Mice were fed with the standard mouse chow (D03 SAFE; Augy, France) and tap water. The different α,25$(OH)_2D_3$ agonists were dissolved in sesame oil and administered intraperitoneally every other day at the indicated doses. Mice were fasted 4 hr prior to blood harvest, and subsequent calcium measurements were determined with a kit supplied by

Olympus according to the manufacturer's procedure on an Olympus AU400 analyzer (Olympus SA, Ringis, France) (Champy et al., 2004).

ACCESSION NUMBERS

The atomic coordinates and structure factors for VDR-AMCR277A and VDR-AMCR277B have been deposited in the Protein Data Bank under ID codes 3CS4 and 3CS6, respectively.

SUPPLEMENTAL DATA

Supplemental Data include two figures and Supplemental Experimental Procedures and can be found with this article online at http://www.chembiol.com/cgi/content/full/15/4/383/DC1/.

ACKNOWLEDGMENTS

We are grateful to A. Steinmeyer (Schering AG) for the gift of 1α,25(OH)$_2$D$_3$. We thank S. Duclaud, C. Haby, and M.F. Champy for excellent technical assistance, the beamline staff at the ESRF (Grenoble, France) for help during data collection, and Dr. I. Robert for flow cytometry data analysis. The study described here was supported by CNRS, INSERM, ULP, the European Commission SPINE (contract QLG2-CT-220-0098) and SPINE2-complexes (contract-no LSHG-CT-2006-031220) under the RDT program "Quality of Life and Management of Living Resources," and the Spanish MEC (grant SAF2004-01885). L.C. thanks the USC for a fellowship. S.H. and P.A. performed research, interpreted data, and wrote the paper. L.C.R. and A.M. performed the synthetic chemistry. B.R.-S.-M., F.C., and B.C.M. performed biological experiments. K.S. interpreted data. N.R. and D.M. designed the study, interpreted data, and wrote the paper. The authors declare that they have no conflicting financial interests.

Received: July 23, 2007
Revised: February 20, 2008
Accepted: March 7, 2008
Published: April 18, 2008

REFERENCES

Banerjee, P., and Chatterjee, M. (2003). Antiproliferative role of vitamin D and its analogs—a brief overview. Mol. Cell. Biochem. *253*, 247–254.

Bouillon, R., Verlinden, L., Eelen, G., De Clercq, P., Vandewalle, M., Mathieu, C., and Verstuyf, A. (2005). Mechanisms for the selective action of vitamin D analogs. J. Steroid Biochem. Mol. Biol. *97*, 21–30.

Bouillon, R., Eelen, G., Verlinden, L., Mathieu, C., Carmeliet, G., and Verstuyf, A. (2006). Vitamin D and cancer. J. Steroid Biochem. Mol. Biol. *102*, 156–162.

Bourguet, W., Ruff, M., Chambon, P., Gronemeyer, H., and Moras, D. (1995). Crystal structure of the ligand-binding domain of the human nuclear receptor RXR-α. Nature *375*, 377–382.

Brünger, A.T., Adams, P.D., Clore, G.M., DeLano, W.L., Gros, P., Grosse-Kunstleve, R.W., Jiang, J.S., Kuszewski, J., Nilges, M., Pannu, N.S., et al. (1998). Crystallographic & NMR system: a new software suite for macromolecular structure determination. Acta Crystallogr. D Biol. Crystallogr. *54*, 905–921.

Campbell, M.J., and Adorini, L. (2006). The vitamin D receptor as a therapeutic target. Expert Opin. Ther. Targets *10*, 735–748.

Carlberg, C., and Dunlop, T.W. (2006). The impact of chromatin organization of vitamin D target genes. Anticancer Res. *26*, 2637–2645.

Champy, M.F., Selloum, M., Piard, L., Zeitler, V., Caradec, C., Chambon, P., and Auwerx, J. (2004). Mouse functional genomics requires standardization of mouse handling and housing conditions. Mamm. Genome *15*, 768–783.

Cheskis, B.J., Freedman, L.P., and Nagpal, S. (2006). Vitamin D receptors ligands for osteoporosis. Curr. Opin. Investig. Drugs *7*, 906–911.

Ciesielski, F., Rochel, N., and Moras, D. (2007). Adaptability of the vitamin D nuclear receptor to the synthetic ligand Gemini: remodelling the LBP with one side chain rotation. J. Steroid Biochem. Mol. Biol. *103*, 235–242.

Ebert, R., Schütze, N., Adamski, J., and Jakob, F. (2006). Vitamin D signaling is modulated on multiple levels in health and disease. Mol. Cell. Endocrinol. *248*, 149–159.

Eelen, G., Verlinden, L., Rochel, N., Claessens, F., De Clercq, P., Vandewalle, M., Tocchini-Valentini, G., Moras, D., Bouillon, R., and Verstuyf, A. (2005). Superagonistic action of 14-epi-analogs of 1,25-dihydroxyvitamin D explained by vitamin D receptor-coactivator interaction. Mol. Pharmacol. *67*, 1566–1573.

El-Kabbani, O., Rogniaux, H., Barth, P., Chung, R.P.-T., Fletcher, E.V., Van Dorsselear, A., and Podjarny, A. (2000). Aldose and aldehyde reductases: correlation of molecular modeling and mass spectrometric studies on the binding of inhibitors to the active site. Proteins *41*, 407–414.

Elstner, E., Linker-Israeli, M., Said, J., Umiel, T., de Vos, S., Shintaku, I.P., Heber, D., Binderup, L., Uskokovic, M., and Koeffler, H.P. (1995). 20-epi-vitamin D3 analogues: a novel class of potent inhibitors of proliferation and inducers of differentiation of human breast cancer cell lines. Cancer Res. *55*, 2822–2830.

Elstner, E., Linker-Israeli, M., Umiel, T., Le, J., Grillier, I., Said, J., Shintaku, I.P., Krajewski, S., Reed, J.C., Binderup, L., et al. (1996). Combination of a potent 20-epi-vitamin D3 analogue (KH1060) with 9-cis-retinoic acid irreversibly inhibits clonal growth, decreases bcl-2 expression, and induces apoptosis in HL-60 leukemic cells. Cancer Res. *56*, 3570–3576.

Fernández, B., Martínez-Perez, J.A., Granja, J.R., Castedo, L., and Mouriño, A. (1992). Synthesis of hydrindan derivatives related to vitamin D. J. Org. Chem. *57*, 3173–3178.

Holick, M.F. (2003). Vitamin D: a millenium perspective. J. Cell. Biochem. *88*, 296–307.

Hourai, S., Fujishima, T., Kittaka, A., Suhara, Y., Takayama, H., Rochel, N., and Moras, D. (2006). Probing a water channel near the A-ring of receptor-bound 1α,25-dihydroxyvitamin D3 with selected 2α-substituted analogues. J. Med. Chem. *49*, 5199–5205.

Jones, T.A., Zou, J.Y., Cowan, S.W., and Kjeldgaard, M. (1991). Improved methods for building protein models in electron density maps and the location of errors in these models. Acta Crystallogr. A *47*, 110–119.

Kabat, M.M., and Radinov, R. (2001). The practical synthesis of vitamin D analogs: a challenge for process research. Curr. Opin. Drug Discov. Devel. *4*, 808–833.

Laudet, V., and Gronemeyer, H. (2002). The Nuclear Receptor Facts Book (London: Academic Press).

Lonard, D.M., and O'Malley, B.W. (2006). The expanding cosmos of nuclear receptor coactivators. Cell *125*, 411–414.

Lythgoe, B. (1980). Synthetic approaches to vitamin D and its relatives. Chem. Soc. Rev. *9*, 449–475.

McCarthy, D.M., San Miguel, J.F., Freake, H.C., Green, P.M., Zola, H., Catovsky, D., and Goldman, J.M. (1983). 1,25-dihydroxyvitamin D3 inhibits proliferation of human promyelocytic leukaemia (HL60) cells and induces monocyte-macrophage differentiation in HL60 and normal human bone marrow cells. Leuk. Res. *7*, 51–55.

Mouriño, A., Torneiro, M., Vitale, C., Fernández, S., Pérez-Sestelo, J., Anné, S., and Gregorio, C. (1997). Efficient and versatile synthesis of A-ring precursors of 1α,25-dihydroxy-vitamin D$_3$ and analogues. Application to the synthesis of Lythgoe-Roche phosphine oxide. Tetrahedron Lett. *38*, 4713–4716.

Nagpal, S., Na, S., and Rathnachalam, R. (2005). Noncalcemic actions of vitamin D receptors ligands. Endocr. Rev. *26*, 662–687.

Norman, A.W., Mizwicki, M.T., and Norman, D.P. (2004). Steroid-hormone rapid actions, membrane receptors and a conformational ensemble model. Nat. Rev. Drug Discov. *3*, 27–41.

Onate, S.A., Tsai, S.Y., Tsai, M.J., and O'Malley, B.W. (1995). Sequence and characterization of a coactivator for the steroid hormone receptor superfamily. Science *270*, 1354–1357.

Otwinowski, Z., and Minor, W. (1997). Processing of X-ray data collected in oscillation mode. Methods Enzymol. *276*, 307–326.

Pakkala, S., de Vos, S., Elstner, E., Rude, R.K., Uskokovic, M., Binderup, L., and Koeffler, H.P. (1995). Vitamin D3 analogs: effect on leukemic clonal growth and differentiation, and on serum calcium levels. Leuk. Res. *19*, 65–72.

Peleg, S., Sastry, M., Collins, E.D., Bishop, J.E., and Norman, A.W. (1995). Distinct conformational changes induced by 20-epi analogues of 1α,25-dihydroxyvitamin D3 are associated with enhanced activation of the vitamin D receptor. J. Biol. Chem. *270*, 10551–10558.

Rachez, C., Lemon, B.D., Suldan, Z., Bromleigh, V., Gamble, M., Näär, A.M., Erdjument-Bromage, H., Tempst, P., and Freedman, L.P. (1999). Ligand-dependent transcription activation by nuclear receptors requires the DRIP complex. Nature *398*, 824–828.

Reddy, G.S., Robinson, M., Wang, G., Palmore, G.T., Gennaro, L., Vouros, P., De Clercq, P., Vandewalle, M., Young, W., Ling, S., et al. (2007). Removal of C-ring from the CD-ring skeleton of 1α,25-dihydroxyvitamin D3 does not alter its target tissue metabolism significantly. Arch. Biochem. Biophys. *460*, 254–261.

Renaud, J.P., Rochel, N., Ruff, M., Vivat, V., Chambon, P., Gronemeyer, H., and Moras, D. (1995). Crystal structure of the RAR-γ ligand-binding domain bound to all-*trans* retinoic acid. Nature *378*, 681–689.

Rochel, N., and Moras, D. (2006). Ligand binding domain of vitamin D receptors. Curr. Top. Med. Chem. *6*, 1229–1241.

Rochel, N., Wurtz, J.M., Mitschler, A., Klaholz, B., and Moras, D. (2000). The crystal structure of the nuclear receptor for vitamin D bound to its natural ligand. Mol. Cell *5*, 173–179.

Rochel, N., Tocchini-Valentini, G., Egea, P.F., Juntunen, K., Garnier, J.M., Vihko, P., and Moras, D. (2001). Functional and structural characterization of the insertion region in the ligand binding domain of the vitamin D nuclear receptor. Eur. J. Biochem. *268*, 971–979.

Rogniaux, H., Van Dorsselaer, A., Barth, P., Biellmann, J.F., Barbanton, J., van Zandt, M., Chevrier, B., Howard, E., Mitschler, A., Potier, N., et al. (1999). Binding of aldose reductase inhibitors: correlation of crystallographic and mass spectrometric studies. J. Am. Soc. Mass Spectrom. *10*, 635–647.

Tocchini-Valentini, G., Rochel, N., Wurtz, J.M., Mitschler, A., and Moras, D. (2001). Crystal structures of the vitamin D receptor complexed to superagonist 20-epi ligands. Proc. Natl. Acad. Sci. USA *98*, 5491–5496.

Tocchini-Valentini, G., Rochel, N., Wurtz, J.M., and Moras, D. (2004). Crystal structures of the vitamin D nuclear receptor liganded with the vitamin D side chain analogues calcipotriol and seocalcitol, receptor agonists of clinical importance. Insights into a structural basis for the switching of calcipotriol to a receptor antagonist by further side chain modification. J. Med. Chem. *47*, 1956–1961.

Vagin, A., and Teplyakov, A. (2000). An approach to multi-copy search in molecular replacement. Acta Crystallogr. D Biol. Crystallogr. *56*, 1622–1624.

Vanhooke, J.L., Benning, M.M., Bauer, C.B., Pike, J.W., and DeLuca, H.F. (2004). Molecular strucutre of the rat vitamin D receptor ligand binding domain complexed with 2-carbon-substituted vitamin D3 hormone analogues and a LXXLL-containing coactivator peptide. Biochemistry *43*, 4101–4110.

Verlinden, L., Verstuyf, A., Van Camp, M., Marcelis, S., Sabbe, K., Zhao, X.Y., De Clercq, P., Vandewalle, M., and Bouillon, R. (2000). The novel 14-Epi-analogues of 1,25-dihydroxyvitamin D3 inhibit the growth of human breast cancer cells in vitro and in vivo. Cancer Res. *60*, 2673–2679.

White, S.L., Belov, L., Barber, N., Hodgkin, P.D., and Christopherson, R.I. (2005). Immunophenotypic changes induced on human HL60 leukaemia cells by 1α,25-dihydroxyvitamin D3 and 12-O-tetradecanoyl phorbol-13-acetate. Leuk. Res. *29*, 1141–1151.

Yamada, S., Shimizu, M., and Yamamoto, K. (2003). Structure-function relationships of vitamin D including ligand recognition by the vitamin D receptor. Med. Res. Rev. *23*, 89–115.

 ©2008 Elsevier Ltd All rights reserved